Nuclear Magnetic Resonance Studies of Convection in the 1,4-Cyclohexanedione−Bromate−Acid Reaction

Melanie M. Britton[†]

Magnetic Resonance Research Centre, Department of Chemical Engineering, University of Cambridge, New Museums Site, Pembroke Street, Cambridge, CB2 3RA, UK

Received: November 9, 2005; In Final Form: February 28, 2006

The manifestation and development of convection during pattern formation in the 1,4-cyclohexanedione−acid−bromate reaction was investigated using pulsed gradient spin−echo nuclear magnetic resonance (PGSE NMR) experiments. An apparatus was devised that enabled convection to be probed inside an NMR spectrometer and prevented hydrodynamic motion arising from extraneous sources, such as poor mixing or temperature gradients imposed by the experimental setup. PGSE experiments were performed concurrently with magnetic resonance imaging (MRI) experiments to show that convection arose spontaneously from inhomogeneities associated with the chemical patterns. Quantitative data on diffusion coefficients and hydrodynamic velocities are reported.

Introduction

Traveling waves can form in reactions where autocatalysis couples with diffusion. In the iodate−arsenous acid,[1] iron(II)−nitric acid[2], and chlorite−tetrathionite[3] reactions, single traveling fronts are observed. Alternatively, in the Belousov−Zhabotinsky[4] (BZ) and 1,4-cyclohexanedione−acid−bromate[5] (CHD) reactions, multiple waves are observed, which can form target patterns or spiral waves.[6] Investigations of the waves and patterns formed in these systems are now frequently undertaken in a gel matrix to suppress convection. Chemically induced convection can be set up by changes in chemical composition or thermal gradients, which in turn produce density gradients, leading to either Bénard-type convection or, where there are local changes in surface tension, Marangoni-type convection.

The overall change in density ($\Delta\rho$) is a sum of compositional ($\Delta\rho_C$) and thermal ($\Delta\rho_T$) density differences.[7] When fluid of greater density is above fluid of lesser density, convection may occur, depending on the magnitude of the density gradient, the radius (r) of the vessel containing the fluid, the kinematic viscosity (μ) and thermal diffusivity (κ) of the fluid, and the average diffusion coefficient (D) of molecules. A measure of the stability of a system is provided by the Rayleigh number,[7] and convection will occur if this number exceeds a critical value, which, in the case of a cylinder,[8] is 67.9. When solute and temperature differences are present, the combined Rayleigh number for a vertical cylinder is defined as[7]

$$\mathrm{Ra} = \frac{r^4 \boldsymbol{g}}{\mu}\left(\frac{1}{\kappa}\frac{\mathrm{d}\rho_T}{\mathrm{d}z} + \frac{1}{D}\frac{\mathrm{d}\rho_C}{\mathrm{d}z}\right) \quad (1)$$

where $\boldsymbol{g}$ is the gravitational acceleration, and dz is the width of the wave front.

Convective effects on chemical waves have been observed in a number of reactions[1−3,9]. Chemical waves produced during the iodate oxidation of arsenous acid are found to propagate more rapidly upward than downward. In this example, the reaction is exothermic and is also accompanied with an isothermal increase in volume during the reaction. The result is that the thermal and compositional changes in density are both positive. So for a descending wave, the reacted solution (which is less dense) is above the unreacted solution, and therefore no convection occurs, as this is a stable configuration. However, for ascending waves, the more dense solution is above the less dense solution and, as this is an unstable configuration, convection occurs. This type of behavior is known as *simple convection*,[1] and the velocity of the wave becomes a superposition of fluid flow and reaction−diffusion velocities. More complicated hydrodynamic effects are observed in the iron(II)−nitric acid chemical wave,[2] where both descending and ascending waves are influenced by hydrodynamics. The behavior observed in this system is known as *multicomponent convection* and arises because $\Delta\rho_C$ and $\Delta\rho_T$ have opposite signs.

Convection in systems with multiple fronts is less well studied. The effect of hydrodynamics on wave fronts has been observed in the BZ reaction[10,11] and in the CHD[12] reaction. There are difficulties with measuring convection in the BZ reaction because carbon dioxide bubbles form, which rise and mix the solution. This problem is overcome in the CHD reaction, where no bubbles are produced. In both systems, the velocity of waves has been found to be dependent on the direction of the wave, with ascending waves being accelerated because of hydrodynamic flow. In these experiments, the presence of convection was measured through visualization of the wave and observing its influence on wave shape and velocity. The behavior of hydrodynamic flow in the BZ reaction has also been the subject of theoretical work.[13−16] Simulations by Vasquez and co-workers[15−17] looked at the onset of convection and predicted traveling convective rolls about the wave interface, which has also been found by Armstrong et al.[13,14]

In addition to buoyancy-driven hydrodynamics, Marangoni convection has been observed in shallow layers of the ferroin-catalyzed BZ reaction.[18−20] In these systems, a periodic change in surface tension is produced at the gas/liquid interface as waves propagate because of the differences in surface tension arising from the two oxidative states of the reaction catalyst. Miike

[†] Present address: School of Chemistry, University of Birmingham, Edgbaston, Birmingham, B15 2TT, UK. E-mail: m.m.britton@bham.ac.uk.

10.1021/jp0564851 CCC: $33.50 © 2006 American Chemical Society
Published on Web 03/28/2006

and co-workers made the first direct measurements of hydrodynamic flow associated with chemical waves using two-dimensional (2D) microscope video imaging. The solution was seeded with polystyrene particles (0.46 μm in diameter), which act as scattering centers for a laser beam. By observing a small region (3 × 3 mm) of the solution under an inverted microscope,[18] they were able to measure the velocity of hydrodynamic flow. It was found that oscillatory surface flow was produced and was responsible for the deformation[18] and acceleration[19,21] of the chemical waves.

To date, two main methods have been used to measure convection. The first measures it through observation of wave shape and velocity and requires that the wave be visualized. Typically, this has been done optically, relying on color differences between the wave and the reaction medium,[10,12] or by using magnetic resonance imaging (MRI),[11] which exploits differences in the NMR relaxation times of the solvent molecules inside the wave and out. Measurement of mass transport is inferred through the behavior of the wave, but not measured directly, and is limited to a region around the wave interface. For a more complete picture of the hydrodynamics associated with chemical waves, a measurement of the fluid surrounding the wave needs to be made, not just at the interface. This has been addressed by the second technique used. The 2D microscope video imaging technique used by Miike and co-workers observed fluid motion around the wave; however, it was restricted to a localized region, and measurements only probed the movement of dispersed particles and were limited to the surface of shallow layers.

This paper presents the first detailed study of the manifestation and development of chemically induced convection using pulsed gradient spin−echo nuclear magnetic resonance (PGSE NMR). This technique is a valuable alternative to the techniques used previously, as it is able to directly measure the displacement of molecules. It is able to monitor the transport behavior of molecules in and around the wave and does not require the system to be seeded with tracer particles. Concurrent PGSE and MRI experiments have been used to investigate the presence of hydrodynamic flow associated with density differences, set up by the formation of chemical waves in the CHD reaction. An important feature of these experiments is the removal of hydrodynamic motion arising from other sources, such as poor mixing or temperature gradients imposed by the experimental setup.

Experimental Section

Magnetic Resonance. For an introduction to the principles of magnetic resonance, the reader is referred elsewhere.[22] The NMR spectrometer used was a Bruker Biospin DMX-300, which comprised a 7.0 T superconducting magnet, operating at a proton resonance frequency of 300 MHz, equipped with shielded and water-cooled gradient coils. All NMR experiments were done at a temperature of 21 ± 0.2 °C, using a 25 mm radio frequency coil. NMR data was analyzed using the software package PROSPA.[23]

Imaging Experiments. Images were obtained using the fast imaging sequence RARE, the details of which can be found elsewhere.[24] This sequence is based on a single-excitation, multiple-echo acquisition, and image contrast is produced through the differences in spin density and T_2 relaxation time differences. Images were made up of 256 × 64 pixel arrays, corresponding to the vertical and horizontal dimensions, with respective fields-of-view of 60 × 30 mm, yielding a pixel size of 234 × 469 μm. In these experiments, the number of echoes collected after each excitation was limited to 16, due to the relatively short T_2 relaxation time of the reacting solution.[25] So, a minimum of four excitations was required, separated by a repetition time of 1 s. Only a single signal average was collected, which meant that each image took 4 s to acquire.

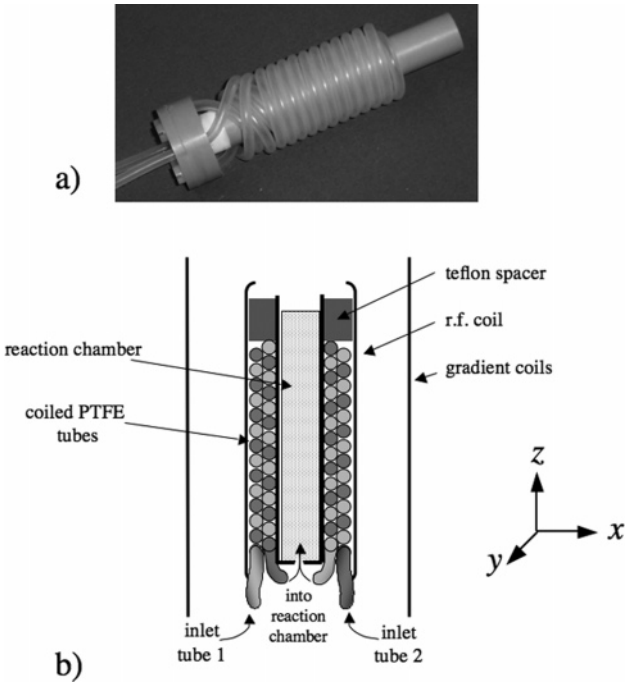

Figure 1. Photo (a) and schematic (b) of convection cell.

Images were produced through detection of the ^{1}H NMR signal of the solvent (predominantly water) molecules. Visualization of the waves was possible through differences in the relaxation time (and hence signal intensity) of water molecules surrounding either the Mn^{2+} or the Mn^{3+} ions. The relaxation time of these molecules is sensitive to the oxidative state of the manganese ions. As Mn^{2+} has more unpaired electrons than Mn^{3+}, it is more paramagnetic, so the relaxation times of water molecules are shorter for those surrounding Mn^{2+} rather than Mn^{3+}. Therefore, in MR images, the signal intensity will be higher in regions where Mn^{3+} ions predominate and will therefore appear brighter.

Chemicals and Apparatus. Two stock solutions were made using reagent grade chemicals, with no further purification, dissolved in 2.5 M sulfuric acid. Solution A contained 0.2 M 1,4-cyclohexanedione (Aldrich) and solution B contained 0.2 M $NaBrO_3$ (Fluka) and 5 × 10^{-4} M $MnSO_4$ (BDH). Stock solutions were made up fresh for each experiment. Each reaction used 1.85 mL of each solution mixed in the reaction vessel inside the MRI spectrometer, producing a reacting solution with the following initial concentrations: $[CHD]_0 = 0.1$ M; $[BrO_3^-]_0 = 0.1$ M; $[Mn^{2+}]_0 = 2.5 \times 10^{-4}$ M; and $[H_2SO_4]_0 = 2.5$ M.

There are a number of external factors which can lead to convection, such as surface evaporative cooling, reagent inhomogeneities, poor mixing, and initial thermal gradients. To investigate purely chemically driven convection, these other factors needed to be removed. To eliminate thermal gradients, introduced when the sample goes from the lab into the MRI spectrometer's magnet, a delivery device, or *convection cell*, (Figure 1) was designed that could store the two stock solutions, separately, inside the spectrometer's imaging probe and magnet. The cell was composed of two poly(tetrafluoroethylene) (PTFE) tubes coiled inside the MRI probe which could hold the two stock solutions separately, prior to their injection into a central

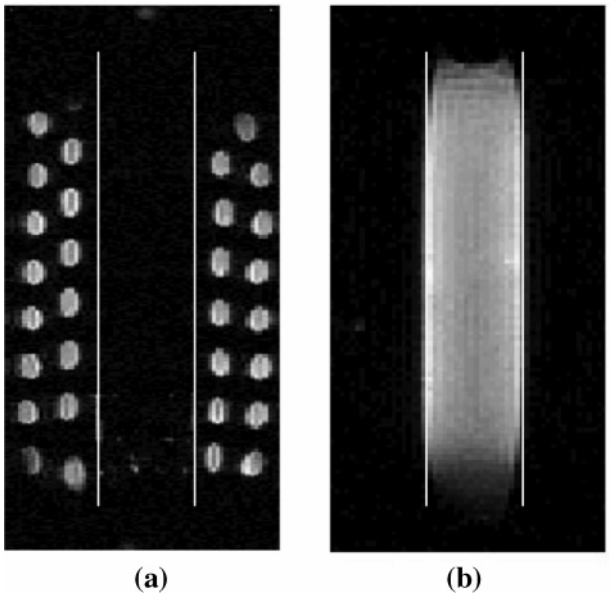

Figure 2. (a) MR image of fluid held inside the two separate PTFE tubes. (b) MR image of fluid inside the central reaction chamber of convection cell, following injection of the fluid and mixing. Both images have 1 mm slice thicknesses and are positioned in the center of the convection cell and have a field-of-view of 60 mm (vertically) × 30 mm (horizontally).

reaction vessel (9 mm i.d.). Because the two stock solutions remained separate, no reaction was initiated. The solutions, however, were contained entirely within the radio frequency (rf) coil, and their temperature was allowed to equilibrate for approximately 20 min before they were injected into the reaction vessel and mixed. The total volume of the reactants was 3.7 mL, which produced a sample height of 58 mm inside the reaction chamber and was contained fully inside the rf coil of the MRI spectrometer. Care was taken to mix the reagents well, and thereby preventing convection associated with inhomogeneities of the reagents.[15] A stopper at the top of the reaction vessel was also used to prevent surface evaporation.

Figure 2a shows MR images of fluid held within the PTFE tubes coiled around the reaction chamber, where the fluid remains before mixing. Figure 2b shows an image of the fluid inside the reaction chamber, immediately after injection and mixing. From the point that the fluid was in the central tube, and well-mixed, MR imaging and PGSE measurements were made.

PGSE Experiments. Measurements of mass transport were made using PGSE NMR experiments, which are explained in detail elsewhere.[22] In these experiments, it is, again, the ^{1}H NMR signal arising from the solvent molecules that is measured. The technique is based on a *spin−echo* and uses a combination of resonant radio frequency pulses and a pair of magnetic field gradient pulses, which phase-encode the NMR signal for translational displacement over a fixed time interval (Δ). Incoherent motion, such as diffusion, will attenuate the NMR signal[26] (echo amplitude) to an extent dependent on the duration (δ) and amplitude (**G**) of the applied magnetic field gradient pulses, the separation between the two pulses (Δ), and the diffusion coefficient of the fluid (D). The echo amplitude is given by

$$E(\mathbf{G}) = \exp[-\gamma^2\mathbf{G}^2\delta^2 D(\Delta - \delta/3)] \qquad (1)$$

where $E(\mathbf{G})$ is the ratio of the echo amplitude at gradient **G** to that at zero gradient, and γ is the gyromagnetic ratio. When diffusion is superposed on flow of velocity v_z, the echo amplitude becomes

$$E(\mathbf{G}) = \exp[-\gamma^2\mathbf{G}^2\delta^2 D(\Delta - \delta/3) + i\gamma\delta\mathbf{G}v_z\Delta] \qquad (2)$$

In these experiments, **G** is varied while Δ and δ are kept constant. Fourier transformation of eq 2 with respect to **q**, where $\mathbf{q} = (2\pi)^{-1}\gamma\mathbf{G}\delta$, produces the propagator, which is a distribution of molecular displacements and can be described by eq 3:

$$P_\Delta(Z,t) = (4\pi Dt)^{-1/2}\exp\{-Z^2 - v_z t/4Dt\} \qquad (3)$$

where Z is the displacement along the direction of the PGSE gradient. Fourier transformation of eq 2 with respect to $\mathbf{q}\Delta$ produces a diffusion-weighted velocity spectrum.[27]

For the PGSE experiments presented in this paper, a PGSE gradient was applied along a vertical (z) direction and ramped from − 0.4 T/m to + 0.4 T/m, over 32 gradient steps. A stimulated echo experiment was performed, which put the NMR magnetization along the longitudinal plane during the displacement time Δ, making the signal dependent on T_1 rather than T_2 relaxation, because T_1 was significantly longer. The observation time (Δ) was 50 ms to minimize any loss in signal due to relaxation, and the duration of the gradient pulses (δ) was 2 ms. Two signal averages were used with a repetition delay of 1 s, which was sufficiently long to allow for T_1 relaxation. The total experiment time for each measurement was 135 s. Measurements of molecular displacement were made periodically once the reactants were mixed, over a period of 45 min, until after wave formation had finished. The appearance of waves was monitored using MRI experiments concurrently, so the point at which waves appeared and disappeared could be monitored.

Results

Figure 3 shows MR images of traveling waves formed at the start of oscillations, after an induction period of approximately 20 min. Multiple excitation sites are apparent, and the formation of well-defined, undistorted waves indicates the absence of convection. This observation is in agreement with PGSE measurements, which returned an apparent diffusion coefficient ($1.42 \pm 0.05 \times 10^{-9}$ m^2 s^{-1}), consistent with that of self-diffusion only. This is a good test that no initial thermal gradients are present and that the system was well mixed.

Undisrupted patterns are not sustained for long, and, soon after they form, they become perturbed, indicating the presence of convection. The development of this convective motion was observed through a series of images taken over a period of 180 s (Figure 4). The first image shows well-resolved waves throughout the observable region of the reaction mixture. Subsequent images, displayed at 20 s intervals, show the waves becoming progressively disrupted. This disruption starts toward the top of the reaction mixture (near the liquid−air interface) and then propagates downward.

The onset of this convection can be followed in more detail using PGSE measurements taken once the reagents were mixed. Figure 5 shows a typical plot of apparent diffusion coefficients, where the displacement-encoding gradient has been directed along the z (vertical) axis. A line is drawn between the points to guide the eye and is not a fit of the data. Images taken between PGSE experiments allowed the start of waves to be detected and is indicated on the plot. For a period of approximately 2200 s after mixing, the apparent diffusion coefficients do not change and are the value expected for self-

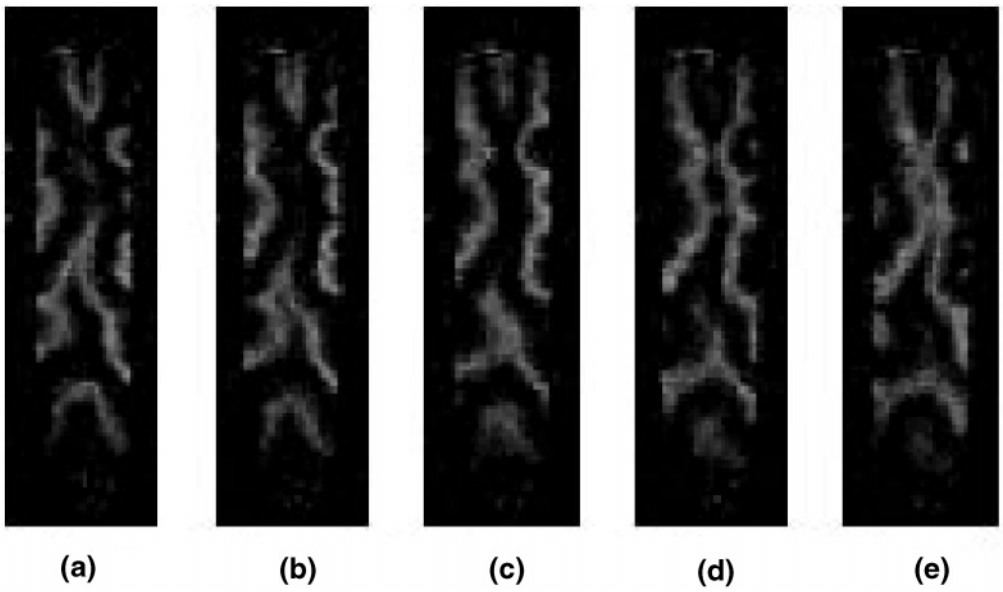

Figure 3. MR images of traveling waves formed during the CHD reaction, taken at the start of pattern formation. A 1 mm slice thickness is used, positioned in the center of the convection cell, and a region of 13.6 mm (horizontally) × 46.7 mm (vertically) is displayed. Images are shown at 4 s intervals.

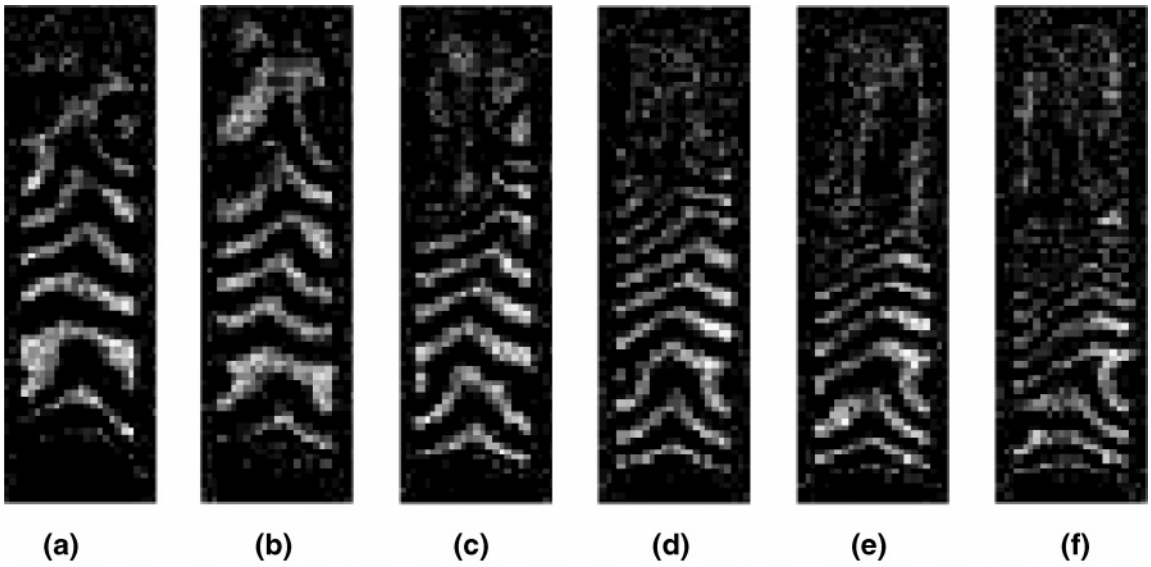

Figure 4. MR images taken at the start of convection. Images are shown at 20 s intervals. Imaging details are the same as those listed for Figure 3.

diffusion in a 2.5 M solution of sulfuric acid ($1.4 \pm 0.1 \times 10^{-9}$ m^2 s^{-1}). Wave formation commences after an induction period of 28 min, and, for a while, there is no enhancement of the diffusion coefficient. The onset of convection is then indicated by the rapid increase in the apparent diffusion coefficient[28] at a point 200−300 s after the formation of waves. The apparent diffusion coefficients increase for a period of 500−700 s until a maximum value of $1.95 \pm 0.1 \times 10^{-9}$ m^2 s^{-1} is reached. After this point, there is a decrease in the apparent diffusion coefficient until it levels off at a value of $1.57 \pm 0.05 \times 10^{-9}$ m^2 s^{-1}.

As this reaction is exothermic, a temperature increase is expected and has been measured at 2.8−3.0 K for this system, from mixing until after wave formation (a period of approximately 45 min). This temperature rise will increase the diffusion coefficient of molecules within the solution, as shown in Figure 6. From this, the diffusion coefficient is expected to go from 1.4×10^{-9} to 1.6×10^{-9} m^2 s^{-1} over the duration of the experiment (approximately 45 min). This steady rise in temperature does not explain, however, the rapid increase in the diffusion coefficient shortly after waves start to form. The explanation for this must be convection. The convection appears to build up to a maximum and remains elevated during wave formation. When no more waves can be observed, the diffusion coefficient then reduces to a constant value that is consistent with the increase in temperature associated with the reaction. An increase of 3.0 K is expected to raise the diffusion coefficient to $1.6 \pm 0.05 \times 10^{-9}$ m^2 s^{-1}, which is in good agreement with what was observed. It should also be noted that measurements of the diffusion coefficient along the x axis (horizontally) D_x showed no significant enhancement during the reaction. This indicates that the enhancement of the diffusion coefficient along the z axis (vertical) D_z is not associated with significant temperature increases, otherwise D_x would be similarly affected.

To ensure that these increases in diffusion coefficients (D_z) were only associated with the reaction, a control experiment was done using a nonreacting solution, composed of 2.5 M of sulfuric acid only, under the same experimental conditions; no

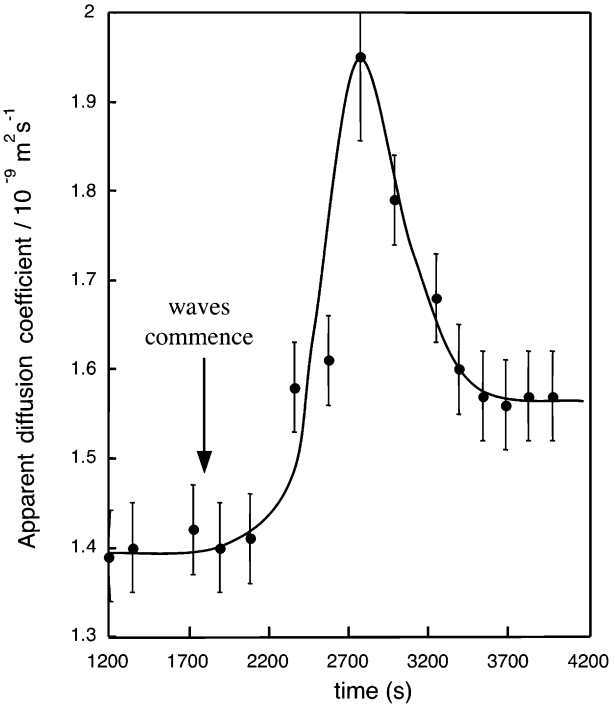

Figure 5. Plot of apparent diffusion coefficient against time.

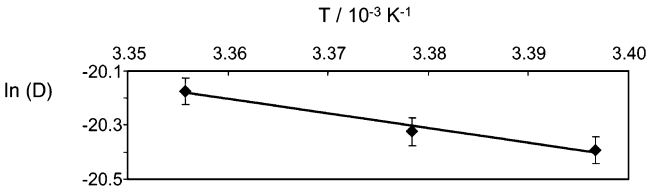

Figure 6. Relationship between the diffusion coefficient (D) and temperature (T) for a solution containing 0.1 M BrO_3^-, 2.5×10^{-4} M $MnSO_4$, and 2.5 M H_2SO_4.

increase in the diffusion coefficient was observed. This shows that the increases in diffusion coefficient are not associated with other external factors.

Discussion

In Pojman and Epstein's analysis of waves in the ferroin-catalyzed BZ reaction,[7] they calculated that convection would occur in tubes of radius 0.1 cm or greater. This was calculated from a density gradient across the wave front of 3.8×10^{-5} g/cm,[4] where the partial molal volume changes had been estimated from the difference in the volumes of solutions containing Fe^{2+} or Fe^{3+} ions. In these calculations, full conversion between the two oxidative states had been assumed. Menzinger et al.[11] studied a manganese-catalyzed BZ[29] reaction and predicted convection would occur in a tube of diameter 0.19 cm or greater, using an estimated density gradient of 4.8×10^{-6} g/cm.[4] In the experiments in this paper, a tube with a larger inner radius (0.45 cm) was used, but it was found that, in these experiments, convection did not commence immediately following the formation of waves.[30] This implies that the density gradient across the wave front is not sufficiently large to initiate convection at the start of pattern formation. This was not too surprising after experiments were performed to probe volume changes during bulk oscillations using a capillary attached to a reaction flask, in which any changes were too small to be detectable. One explanation for this could be that the concentration of manganese was too low to produce observable volume changes. Another possibility is that full conversion did not occur between the two oxidative states of the manganese ion. Indeed, measurements of redox potential for this system show that the amplitude of oscillations increases as the reaction progresses, and this would suggest that the degree of conversion may also increase. This would be consistent with observations, where convection occurs a short time after pattern formation. So maybe, at the start of pattern formation, the degree of conversion is too small to produce sufficient density differences to initiate convection. Then, as the reaction proceeds, the degree of conversion increases, as do the differences in density, leading to convection.

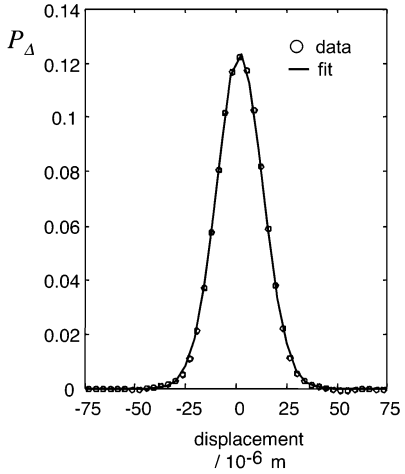

Figure 7. Plot of the normalized distribution of molecular displacement (P_Δ) for a system undergoing self-diffusion only. Fitting the data to a single Gaussian gives a diffusion coefficient (D) of $1.4 \pm 0.05 \times 10^{-9}$ m^2 s^{-1}.

Finally, the PGSE data, used to calculate the apparent diffusion coefficients presented in Figure 5, were reanalyzed to extract the distribution of molecular displacements within the system. These distributions, or propagators (eq 3), were produced by Fourier transforming the echo amplitudes for each PGSE experiment with respect to **q**. For the first five PGSE experiments shown in Figure 5, these distributions were Gaussian in shape and centered about zero, which is consistent with self-diffusion. A typical propagator from these experiments is shown in Figure 7. As the apparent diffusion coefficients start to increase, however, a single Gaussian is no longer sufficient to fit the data. Indeed, when the apparent diffusion coefficient reached a maximum ($t = 2700$ s), two Gaussian components were required to fit the data, as shown in Figure 8. The major component (58.4%) gave an apparent diffusion coefficient of $1.6 \pm 0.1 \times 10^{-9}$ m^2 s^{-1}, and the minor component (41.6%) yielded $4.1 \pm 0.5 \times 10^{-9}$ m^2 s^{-1}. The first component returns a value consistent with self-diffusion. However, it is suggested that the second component represents the velocity distribution for convecting molecules and not a diffusion coefficient. The displacement of the fluid experiencing convection will be a superposition of diffusion and velocity. Diffusion will be uniform, but the velocity of the convecting molecules will be determined by where they are within a convective roll; therefore, there will be a range of velocities, which can be both positive and negative. The exact distribution of these velocities is not known, but it is found here that it can be approximated to a Gaussian function. By removing the component associated with diffusion, it was possible to then extract this velocity distribution (P_v) associated with convection, which is shown in Figure 9. The velocity range shown here is consistent with velocities measured previously in this system at the onset of convection, using a DANTE MRI experiment.[25]

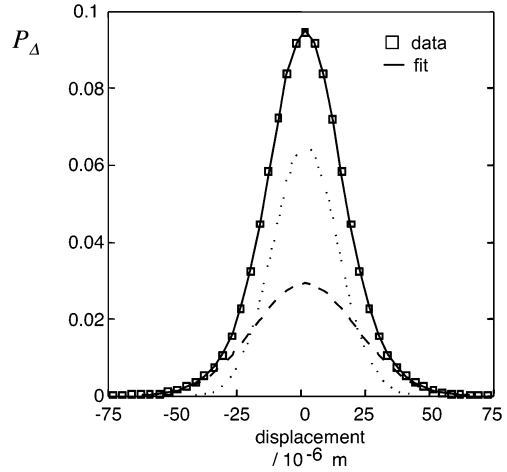

Figure 8. Plot of the normalized distribution of molecular displacement (P_Δ) for a system undergoing self-diffusion and convection. The data can be fitted with two Gaussian functions, where component 1 (dotted line) has a D of $1.6 \pm 0.1 \times 10^{-9}$ m^2 s^{-1}, and component 2 (dashed line) has a D of $4.1 \pm 0.5 \times 10^{-9}$ m^2 s^{-1}.

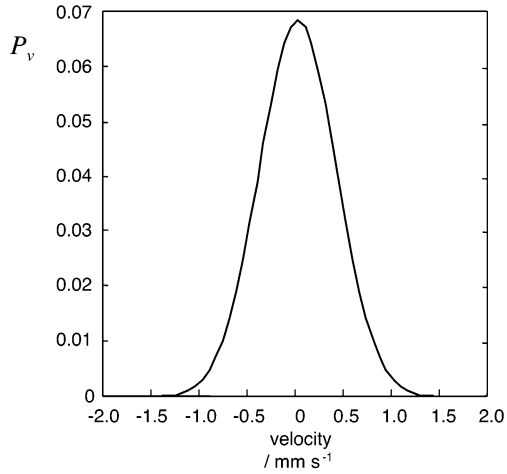

Figure 9. Plot of the normalized velocity distribution (P_v) for the convecting fluid at the maximum apparent diffusion coefficient shown in Figure 7 ($t = 2800$ s).

Following the development of convection, it was found that subsequent propagators could be fitted using a single Gaussian again. This suggested that any coherent motion (flow) had ceased. This agrees with observations made using DANTE MRI experiments[31] following the development of convection, where distortions in the waves were still detected, but not matched with distortions of the applied magnetization grid. This indicates that the waves were not influenced by convective flow anymore. However, these PGSE experiments show that there remains a persistent enhancement of the diffusion coefficient after the initial onset of convection, and that this enhancement is anisotropic, with D_z being greater than D_x. This behavior would not distort the DANTE grid.

Conclusions

These are the first measurements of the onset and development of convection during chemical pattern formation using PGSE NMR experiments. Apparent diffusion coefficients are measured during the CHD reaction and are found to be sensitive to the temperature of the solution and the presence of convection. They show that convective motion builds up to a maximum and then reduces. Analysis of the PGSE data, where the apparent diffusion coefficient was at a maximum, was able to produce a velocity distribution for convecting molecules. Future work will aim to combine the PGSE experiment with a fast-imaging experiment, so that a spatial representation of fluid flow can be produced during convection.

Acknowledgment. M.M.B. thanks EPSRC for an Advanced Research Fellowship, Lynn F. Gladden and her group at the MRRC, Cambridge University, for support, and Desiderio Vasquez for helpful discussions. M.M.B. also thanks the reviewers of this paper for suggestions that have improved this paper.

References and Notes

(1) Pojman, J. A.; Epstein, I. R.; McManus, T. J.; Showalter, K. *J. Phys. Chem.* **1991**, *95*, 1299.
(2) Bazsa, G.; Epstein, I. R. *J. Phys. Chem.* **1985**, *89*, 3050.
(3) Horvath, D.; Bansagi, T.; Toth, A. *J. Chem. Phys.* **2002**, *117*, 4399.
(4) Zaikin, A. N.; Zhabotinsky, A. M. *Nature* **1970**, *225*, 535.
(5) Kurin-Csörgei, K.; Szalai, I.; Körös, E. *React. Kinet. Catal. Lett.* **1995**, *54*, 217.
(6) Epstein, I. R.; Pojman, J. A. *An Introduction to Nonlinear Chemical Dynamics*; Oxford University Press: Oxford, 1998.
(7) Pojman, J. A.; Epstein, I. R. *J. Phys. Chem.* **1990**, *94*, 4966.
(8) Taylor, G. I. *Proc. Phys. Soc., London, Sect. B* **1954**, *67*, 857.
(9) Rodriguez, J.; Vidal, C. *J. Phys. Chem.* **1989**, *93*, 2737.
(10) Fulieda, S.; Mogamia, Y.; Furuya, A.; Zhang, W.; Araiso, T. *J. Phys. Chem. A* **1997**, *101*, 7926.
(11) Menzinger, M.; Tzalmona, A.; Armstrong, R. L.; Cross, A.; Lemaire, C. *J. Phys. Chem.* **1992**, *96*, 4725.
(12) Komlósi, A.; Nagy, I. P.; Bazsa, G.; Pojman, J. A. *J. Phys. Chem. A* **1998**, *102*, 9136.
(13) Zhang, D.; Peltier, W. R.; Armstrong, R. L. *J. Chem. Phys.* **1995**, *103*, 4078.
(14) Zhang, D.; Peltier, W. R.; Armstrong, R. L. *J. Chem. Phys.* **1995**, *103*, 4069.
(15) Wu, Y. Q.; Vasquez, D. A.; Edwards, B. F.; Wilder, J. W. *Phys. Rev. E* **1995**, *51*, 1119.
(16) Masere, J.; Vasquez, D. A.; Edwards, B. F.; Wilder, J. W.; Showalter, K. *J. Phys. Chem.* **1994**, *98*, 6505.
(17) Vasquez, D. A.; Wilder, J. W.; Edwards, B. F. *Phys. Fluids A* **1992**, *4*, 2410.
(18) Miike, H.; Müller, S. C.; Hess, B. *Phys. Rev. Lett.* **1988**, *61*, 2109.
(19) Miike, H.; Yamamoto, H.; Kai, S.; Müller, S. C. *Phys. Rev. E* **1993**, *48*, 1627.
(20) Yoshikawa, K.; Kusumi, T.; Ukitsu, M.; Nakata, S. *Chem. Phys. Lett.* **1993**, *211*, 211.
(21) Kai, S.; Ariyoshi, T.; Inenaga, S.; Miike, H. *Physica D* **1995**, *84*, 269.
(22) Callaghan, P. T. *Principles of Nuclear Magnetic Resonance Microscopy*; Oxford University Press: Oxford, 1991.
(23) PROSPA, Magritek Home Page. http://www.magritek.com/prospa.html (purchased 2005).
(24) Hennig, J.; Naureth, A.; Friedburg, H. *Magn. Reson. Med.* **1986**, *3*, 823.
(25) Britton, M. M. *J. Phys. Chem. A* **2003**, *107*, 5033.
(26) Stejskal, E. O.; Tanner, J. E. *J. Chem. Phys.* **1965**, *42*, 288.
(27) Mao, X.-A.; Kohlmann, O. *J. Magn. Reson.* **2001**, *150*, 35.
(28) Goux, W. J.; Verkruyse, L. A.; Salter, S. J. *J. Magn. Reson.* **1990**, *88*, 609.
(29) Gao, Y.; Cross, A. R.; Armstrong, R. L. *J. Phys. Chem.* **1996**, *100*, 10159.
(30) Although this has been found to be dependent on the height of the solution.
(31) Britton, M. M. Unpublished work, 2004.